Electronic Supplementary Material (ESI) for Energy & Environmental Science.

Supplementary Information for

Structural and Chemical Synergistic Encapsulation of Polysulfides Enables Ultralong-Life Lithium-Sulfur Batteries

Xiaolei Wang,[a] *Ge Li,*[a] *Jingde Li,*[a] *Yining Zhang,*[a] *Ahn Wook,*[a] *Aiping Yu*[a] *and Zhongwei Chen*[a]*

[a] Dr. X. Wang, Dr. G. Li, Dr. J. Li, Dr. Y. Zhang, Dr. A. Wook, Prof. Dr. A. Yu, Prof. Dr. Z. Chen
Department of Chemical Engineering
Waterloo Institute for Nanotechnology and Waterloo Institute for Sustainable Energy
University of Waterloo
200 University Avenue West, Waterloo, Ontario N2L3G1, Canada

**Corresponding authors. E-mail address: zhwchen@uwaterloo.ca (Z. Chen)*

1. METHODS

Synthesis of hollow sulfur-MnO_2 nanosheets spheres:

The hollow S spheres were synthesized according to the literature.[1] In a typical synthesis, sodium thiosulfate ($Na_2S_2O_3$) aqueous solution (80 mM, 50 mL) was mixed with PVP (Mw: ~40,000) aqueous solution (0.4 M, 50 mL) at room temperature. Then, concentrated hydrochloric acid (HCl) (0.4 mL) was added to the above solution under magnetic stirring, and the reaction was allowed to proceed for 2 h. The precipitate was collected by centrifuging at 7000 rpm for 10 min, follow by washing with PVP aqueous solution (0.8 M) once and centrifuging at 6,000 rpm for 15 min. The precipitate was re-dispersed in PVP aqueous solution (0.8 M, 10 mL). For the MnO_2 growth, the homogeneous dispersion (5 mL) was diluted to 20 mL by adding DDI water. Potassium Permanganate ($KMnO_4$) (0.1106 g) was added to the diluted dispersion and the reaction was allowed to proceed for 5 min at 70 ^{o}C under magnetic stirring. The hollow sulfur-MnO_2 nanosheets spheres were obtained after centrifuging and washing by DDI water and ethanol for 5 times followed by naturally drying at room temperature for 2 days.

Synthesis of polysulfide (Li_2S_4) and MnO_2 nanosheets:

The Li_2S_4 was synthesized according to the literature.[2, 3] In a typical synthesis, sulfur was fully dissolved in Super-Hydride Solution (1.0 M lithium triethylborohydride in tetrahydrofuran) in a molar ratio of 2.75:1. The resulting solution was dried under vacuum, and a yellow powder precipitate was obtained. The yellow powder was washed by toluene and isolated by centrifugation for several times to obtain the polysulfide (Li_2S_4) powder.

Synthesis of polysulfide/MnO_2 composites:

The polysulfide/MnO_2 composites were prepared by mixing the two components. The MnO_2 nanosheets were obtained from the hollow S-MnO_2 nanocomposites by removing the sulfur content using carbon disulfide (CS_2) to dissolve and wash. The MnO_2 was dried in vacuum oven before re-dispersed in dimethyl ether (DME). The dispersion was injected into a transparent yellow 1,3-dioxolane (DOL) solution containing polysulfide. The polysulfide/MnO_2 composites were achieved by collecting the precipitates.

Physical and chemical characterization:

Scanning electron microscopy (SEM) was conducted using an LEO FESEM 1530 microscope. Transmission electron microscopy was performed using JEOL 2010F TEM/STEM field emission microscope equipped with a large solid angle for high X-ray throughput, scanning, scanning-transmission and a Gatan imaging filter for energy filtered imaging. X-ray photoelectron spectroscopy (XPS) spectra were collected on a Thermal Scientific *K*-Alpha spectrometer.

Electrode fabrication and testing

A conventional slurry-coating process was used to fabricate the electrodes. The active material powders, Super P conductive agent and poly(vinylidene fluoride) (PVDF) binder were mixed in a mass ratio of 75:15:10, and homogenized in *N*-Methyl-2-pyrrolidone (NMP) to form slurries. The homogenous slurries were uniformly coated on carbon-coated Al foil substrates and dried at 60 ^{o}C for 8 hrs. The mass loading on each electrode was controlled to be 2.3-2.7 mg cm^{-2}, corresponding to S mass loading of 1.7-2.1 mg cm^{-2}. The Li-S battery performance was tested using 2016-type coin cells with lithium discs as the counter electrodes, Celgard 3501 membrane as the separator, and 1.0 M lithium *bis*(-trifluoromethanesulphonyl)imide in 1:1 v/v DOL/DME containing $LiNO_3$ (2 wt%).

Cyclic voltammetric (CV) measurements were carried out on a VSP300 potentiostat/galvanostat (Bio-Logic LLC, Knoxville, TN) using cutoff voltages of 3.0 and 1.5 V *versus* Li/Li$^+$. The galvanostatic charge/discharge measurements were performed on NEWARE BTS-CT3008 (Neware Technology, Ltd., Shenzhen, China) at different current densities. Electrochemical impedance spectroscopy measurement was conducted on a Princeton Applied Research VersaSTAT MC potentiostat. The Nyquist plots were recorded potentiostatically by applying an AC voltage of 10 mV amplitude in the frequency range of 0.01 to 10^5 Hz. All electrochemical measurements were carried out at room temperature.

Computational details:

The DFT calculations were carried out using the program BAND, where the electron wave functions were developed on a basis set of numerical atomic orbitals (NAOs) and Slater type orbitals (STOs).[4] The triple polarization (TZP) basis of Slater-type orbitals was used. The calculations were performed by using PBE generalized gradient approximation (GGA) for the exchange and correlation energy terms.[5] This is a widely used functional for various applications and produces reliable energetics on metal oxide systems.[6, 7] The BAND program performs numerical integrations for all the matrix elements.[8] The accuracy of the integration in real space (Accuracy) and the sampling of the Brillouin zone (KSpace) for the integration accuracy in k-space are two key major numerical parameters in the present DFT calculations. “Accuracy” is a very general accuracy parameter. It determines the generation of integration points, and the values of many other parameters and settings that are related to the accuracy of the results. In the present study, the Accuracy parameter was set to 4, which is a reasonable value.[9] The

"K-Space" parameter was set to 3, which represents that the quadratic tetrahedron method was chosen to perform the k-space numerical integration. The calculations performed on this study were spin-unrestricted.[10, 11]

In the present study, the interaction of various Li_xS_n species with δ-MnO_2 anchoring support was investigated. These Li_xS_n species includes S_8, Li_2S_8, Li_2S_6, Li_2S_4, Li_2S_2 and Li_2S, which represent the critical lithiation stages.[6, 12] In order to describe the interactions between the $Li_{x(x=0,2)}S_n$ and MnO_2, the bonding energies (E_{bind}) of $Li_{x(x=0,2)}S_n$ species were calculated as follows:

$$E_{bind}(Li_xS_n)=E(Li_xS_n\,/MnO_2)-E(Li_xS_n)-E(MnO_2), \qquad (1)$$

A negative E_{bind} corresponds to a stable adsorbate/slab system and indicates that the binding interaction is favored.

The δ-MnO_2 synthesized in this study belongs to the C2/m space group with lattice constants a =5.149 Å, b =2.843 Å, c =7.176 Å.[13] In the present study, The δ-MnO_2 support was modeled by the δ-MnO_2 (100) surface using periodic two–layer slabs with a (2×2) unit cell. The (100) surface was selected because it is one of the most detected and catalytically active surfaces for anchoring deposited particles.[14-16] The bottom atomic layer of the slab was fixed in its bulk positions, whereas the remaining atomic layers and the adsorbed species were set free to relax.

2. FIGURES

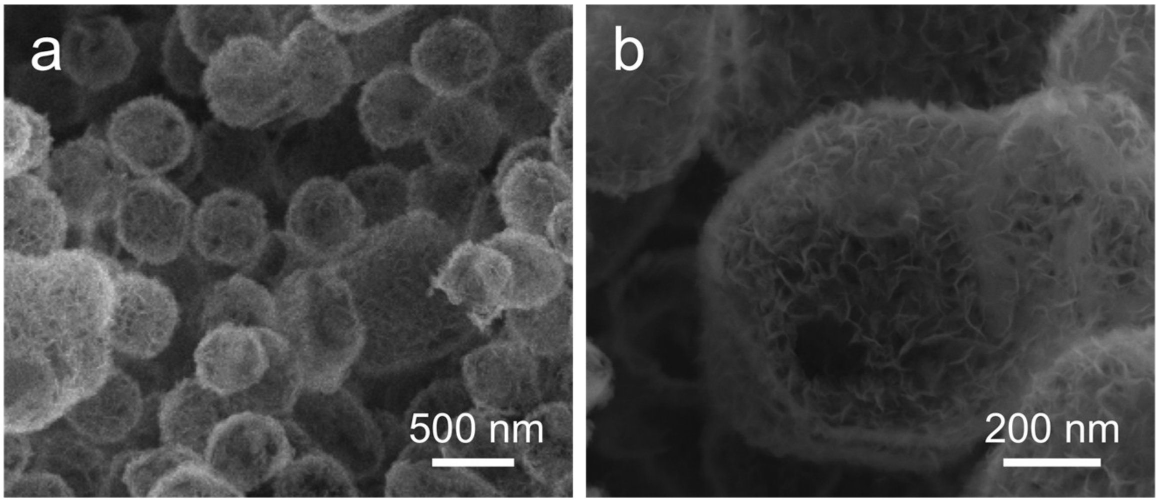

Supplymentary Figure 1. (a) Low- and **(b)** high-magnification SEM images of hollow sulfur-MnO_2 composite spheres.

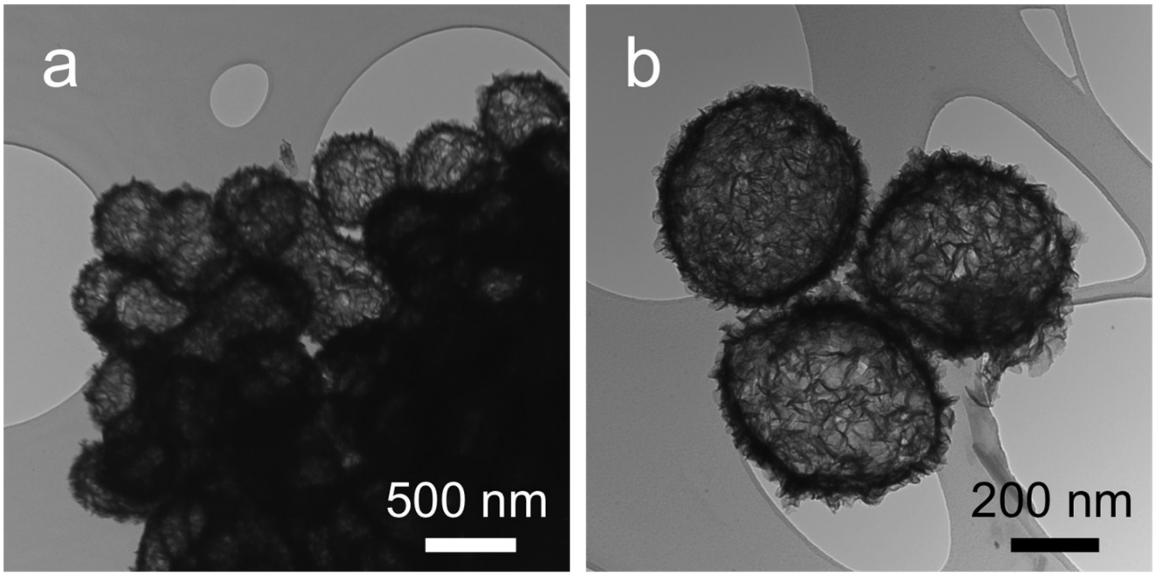

Supplymentary Figure 2. (a) TEM and **(b)** High-magnification TEM images of three hollow sulfur-MnO_2 composite spheres.

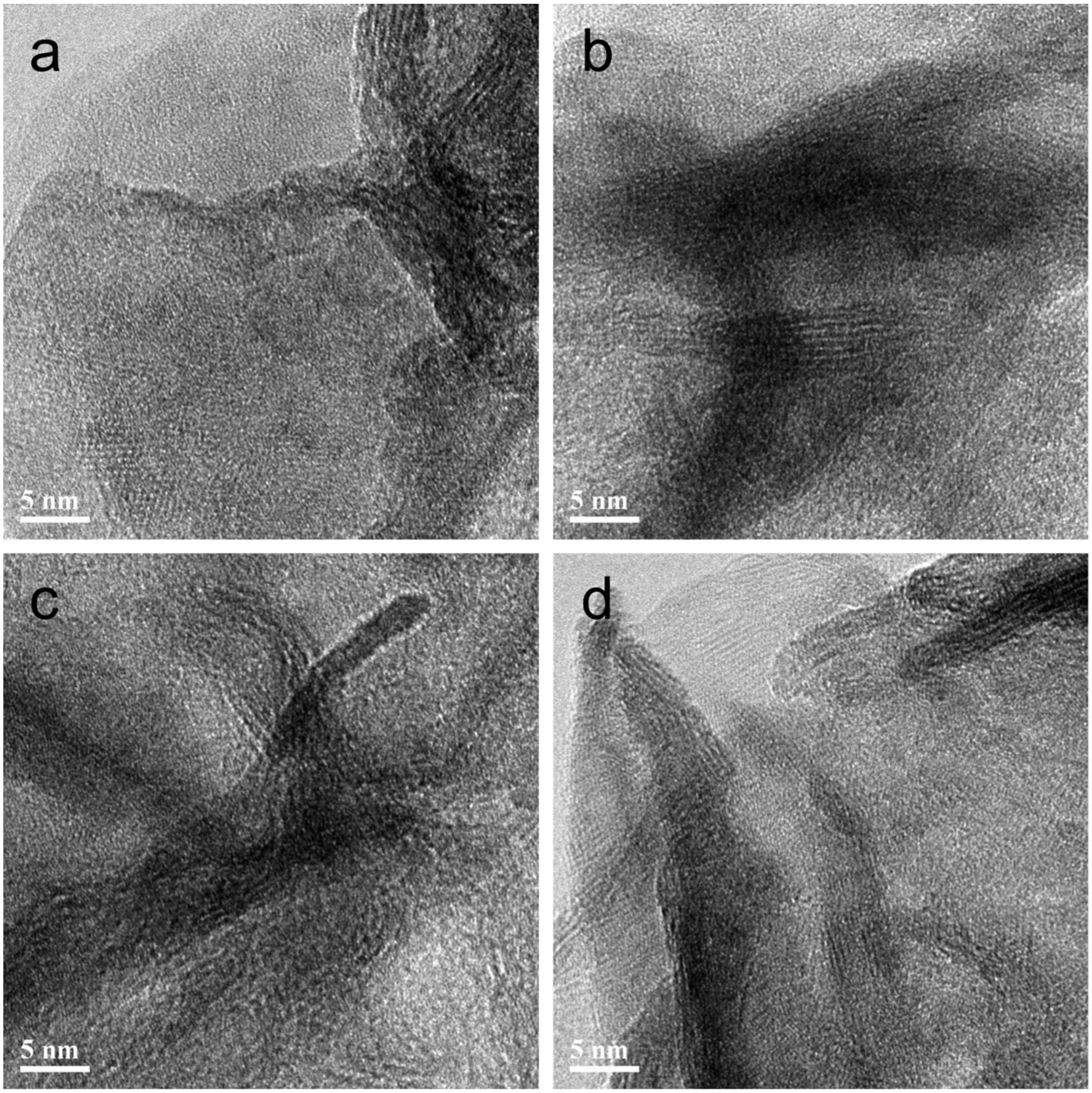

Supplymentary Figure 3. (a-d) HRTEM image of MnO_2 nanosheets from different hollow S-MnO_2 nanocomposite spheres.

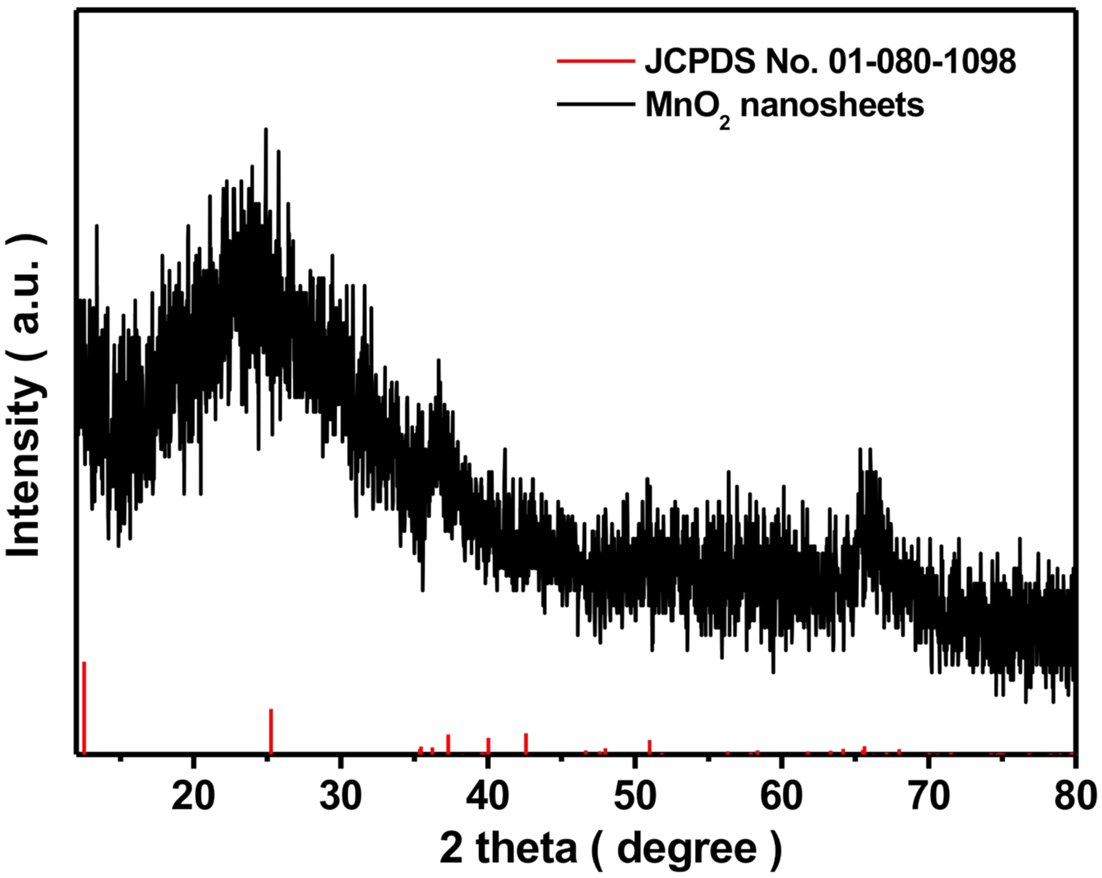

Supplymentary Figure 4. XRD pattern of the MnO_2 nanosheets.

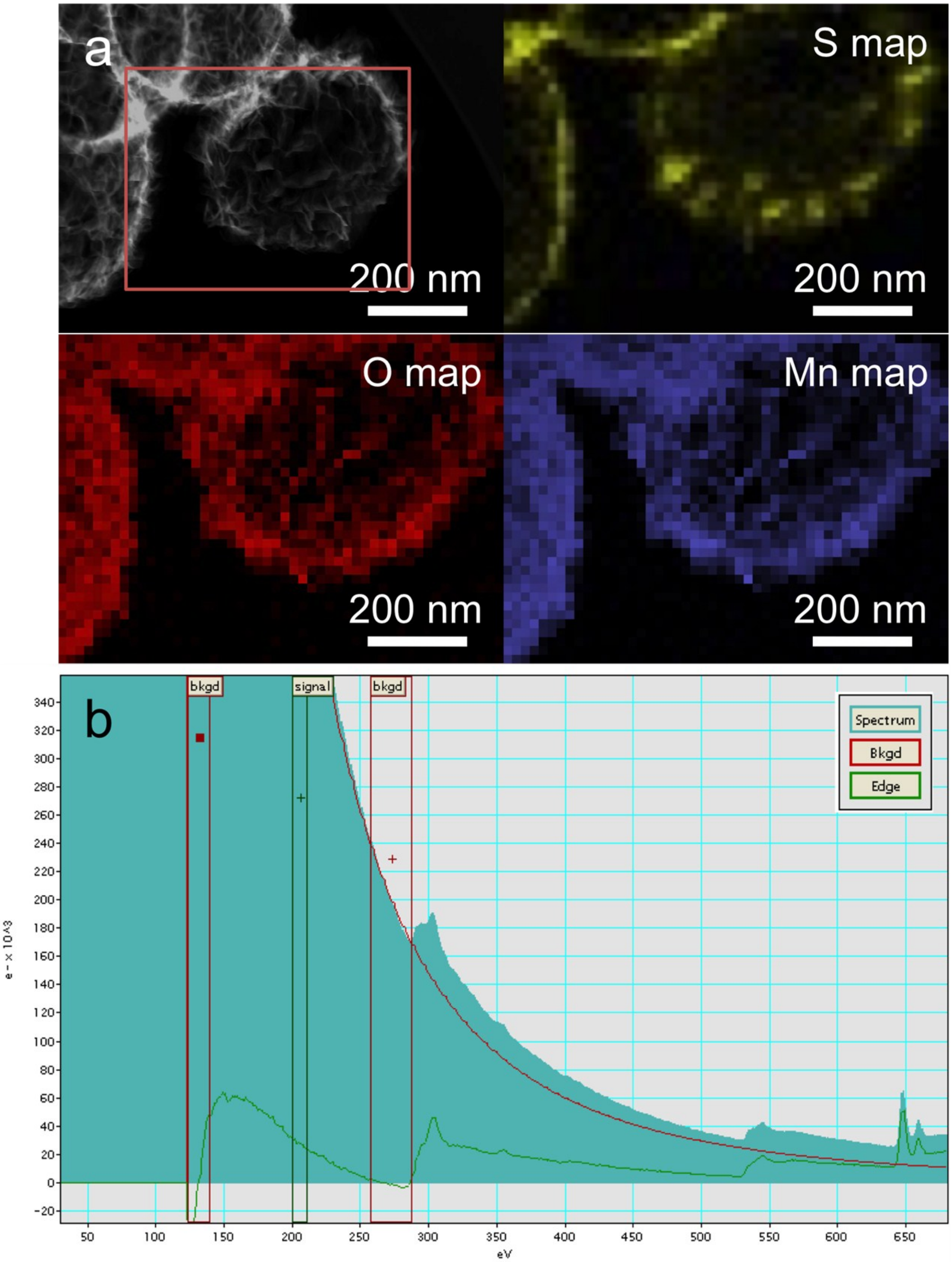

Supplymentary Figure 5. (a) HAADF-STEM image of hollow sulfur-MnO_2 composite spheres and corresponding EELS element mapping. **(b)** EELS spectrum of the hollow sulfur-MnO_2 composite spheres.

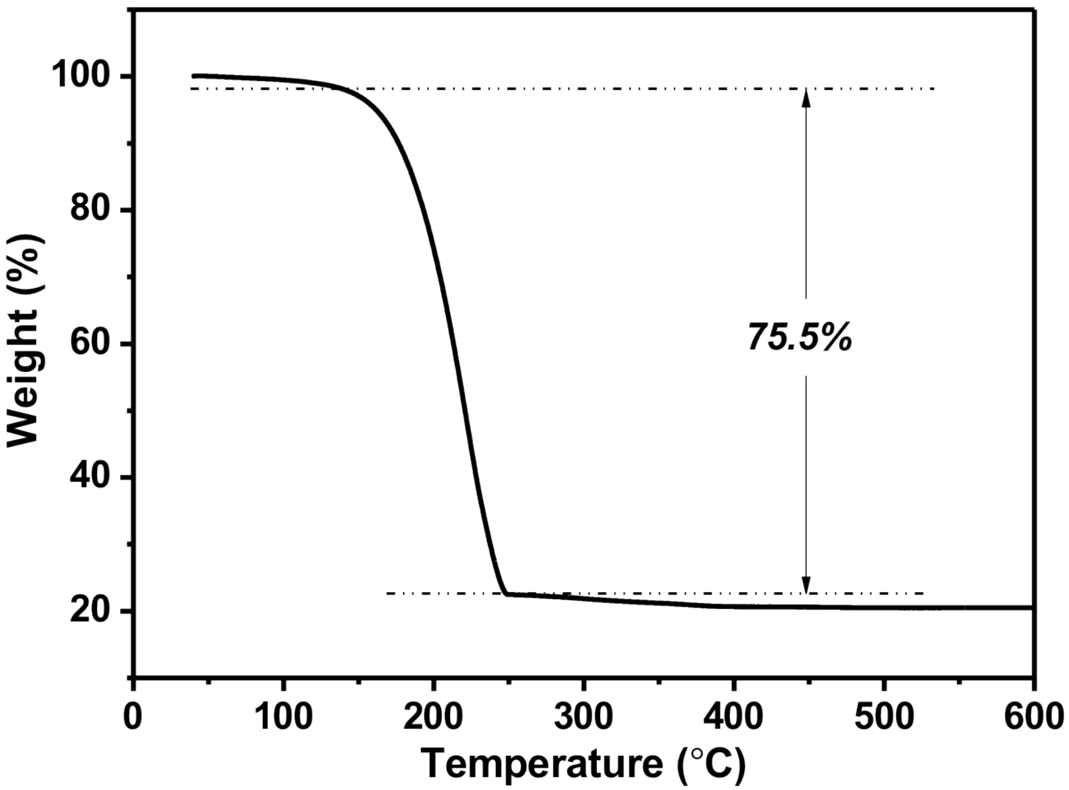

Supplymentary Figure 6. TGA curve of hollow sulfur-MnO_2 nanocomposite spheres.

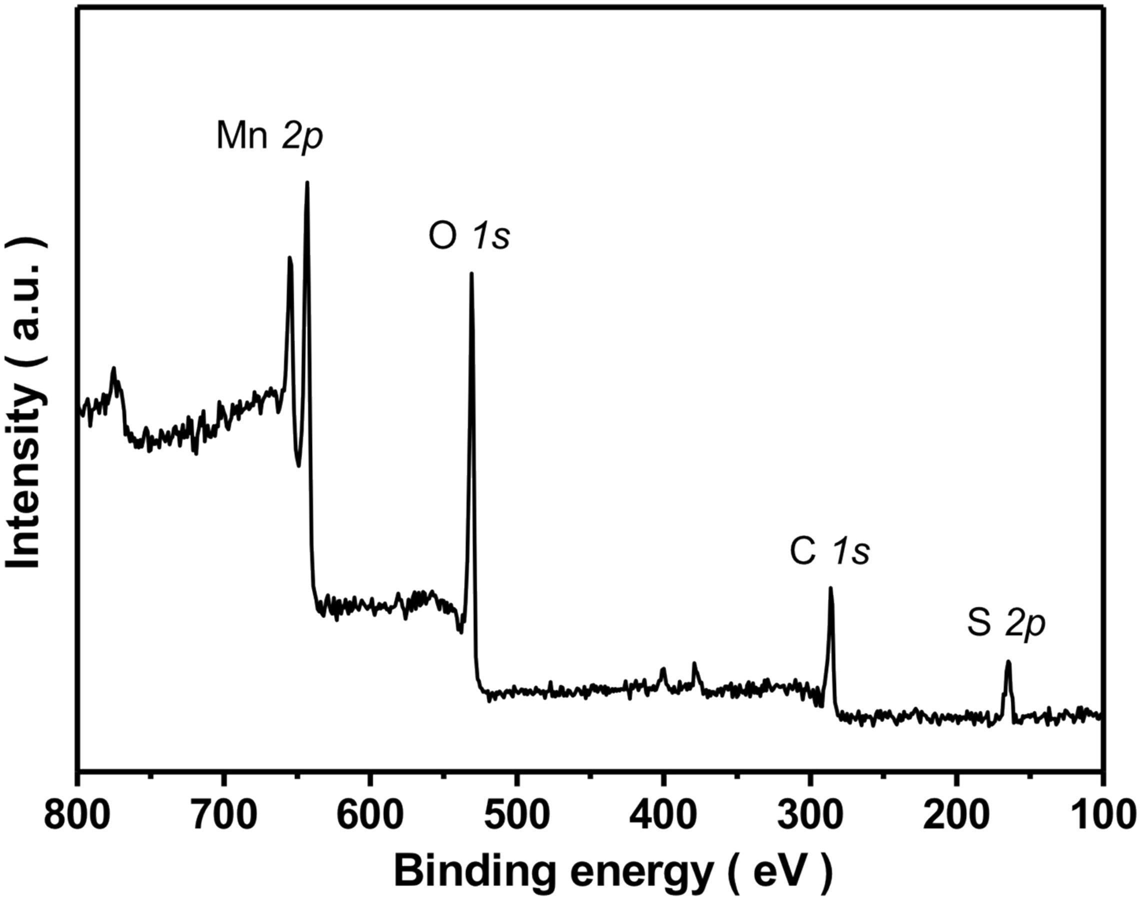

Supplymentary Figure 7. XPS survey-level scan spectrum of the hollow S-MnO_2 nanocomposites.

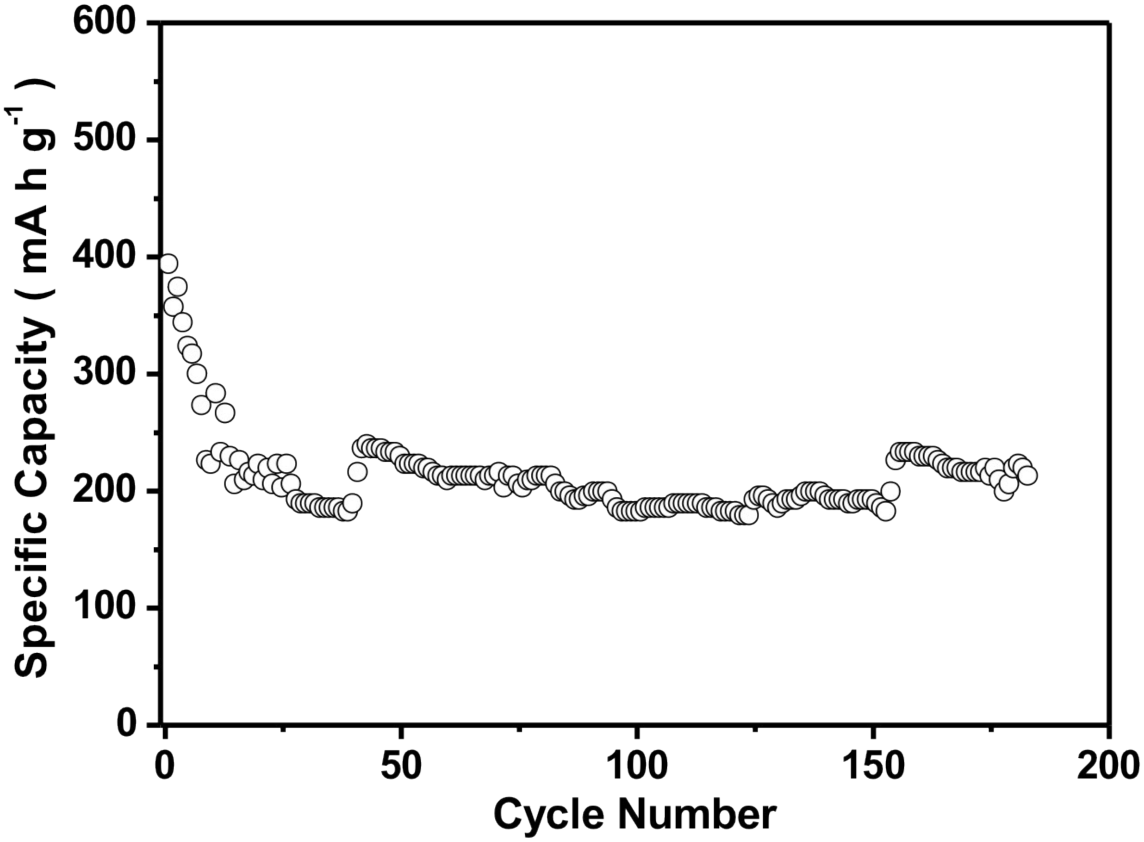

Supplymentary Figure 8. Cycling performance of pure S electrode using commercial S powders as the active material within the voltage window of 1.5-3.0 V *vs.* Li/Li$^+$ in the electrolyte of 1.0 M lithium *bis*(-trifluoromethanesulphonyl)imide in 1:1 v/v DOL/DME containing LiNO3 (2 wt%).

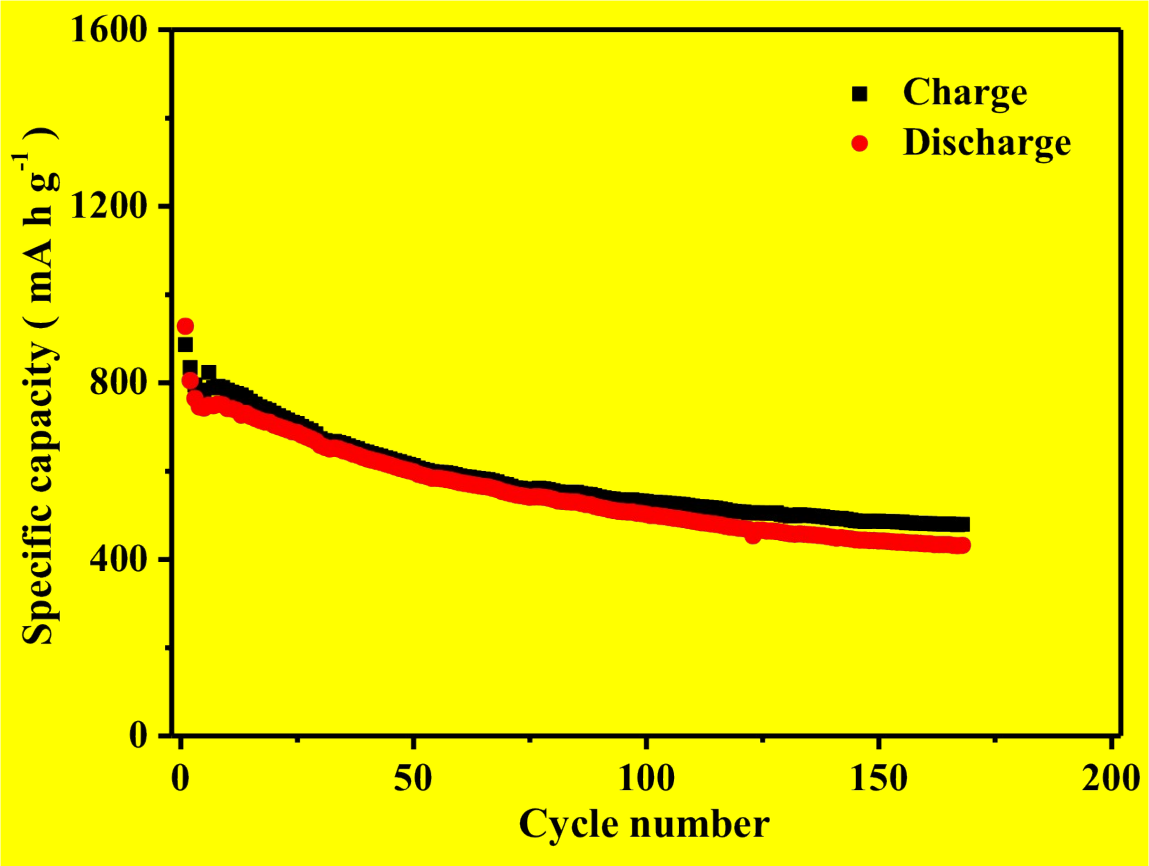

Supplymentary Figure 9. Cycling performance of the composites from simply mixing MnO_2 nanosheets obtained under the same condition and commercial S powders within the voltage window of 1.5-3.0 V *vs.* Li/Li^+ in the electrolyte of 1.0 M lithium *bis*(-trifluoromethanesulphonyl)imide in 1:1 v/v DOL/DME containing LiNO3 (2 wt%).

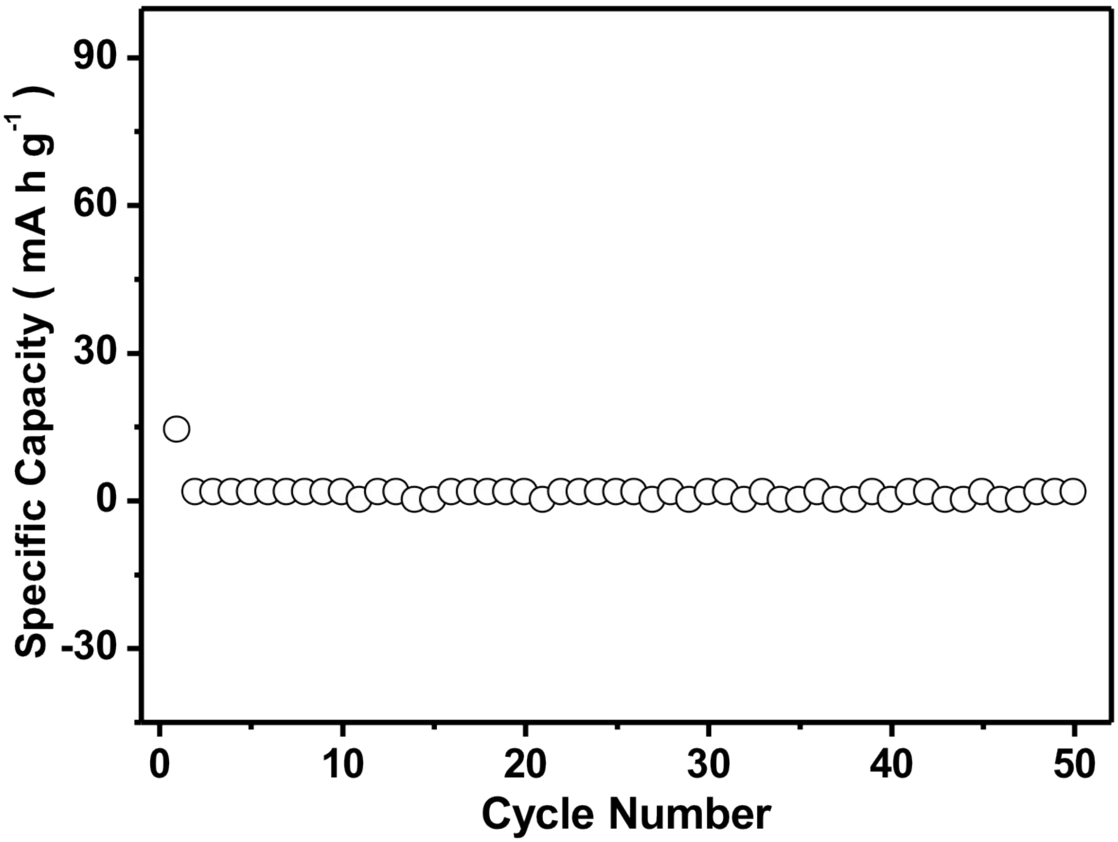

Supplymentary Figure 10. Cycling performance of pure MnO_2 obtained by removing S content from hollow S-MnO_2 nanocomposites within the voltage window of 1.5-3.0 V *vs.* Li/Li^+ in the electrolyte of 1.0 M lithium *bis*(-trifluoromethanesulphonyl)imide in 1:1 v/v DOL/DME containing LiNO3 (2 wt%).

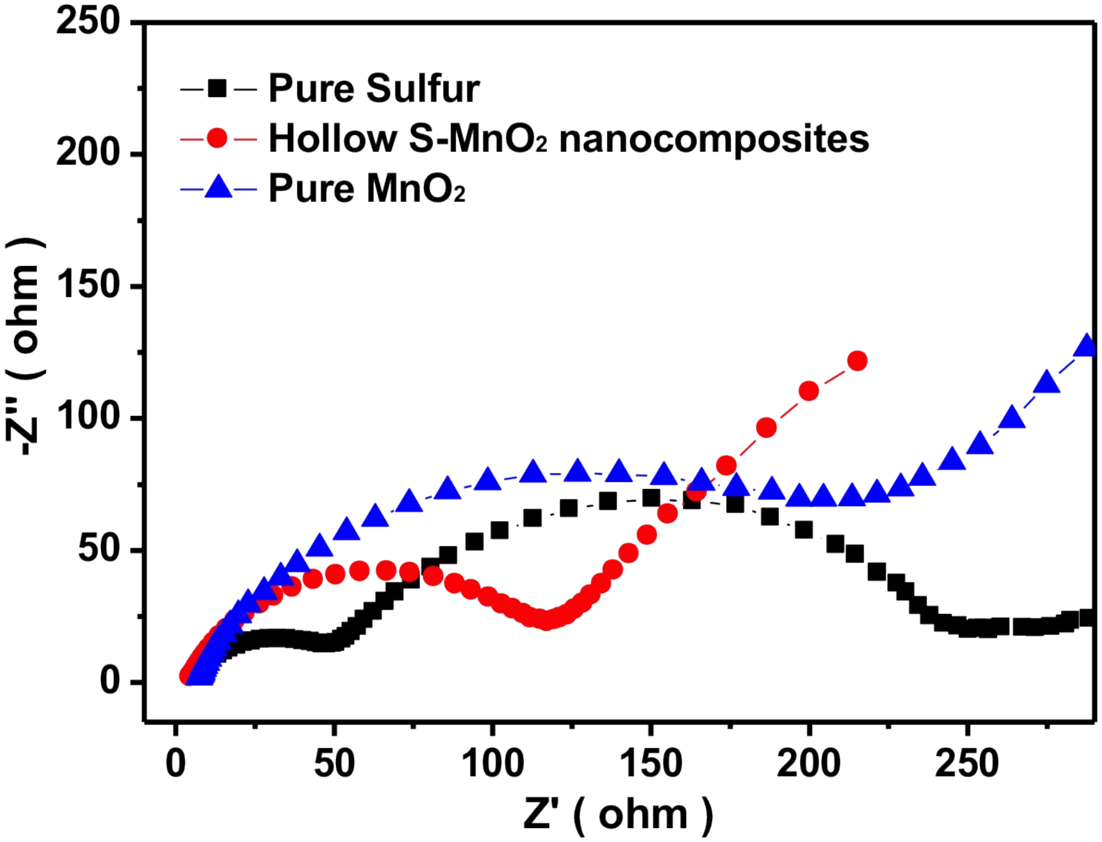

Supplymentary Figure 11. Comparison of Nyquist plots of hollow S-MnO_2 nanocomposites, pure S, and pure MnO_2 obtained by removing the S content in hollow S-MnO_2 nanocomposites.

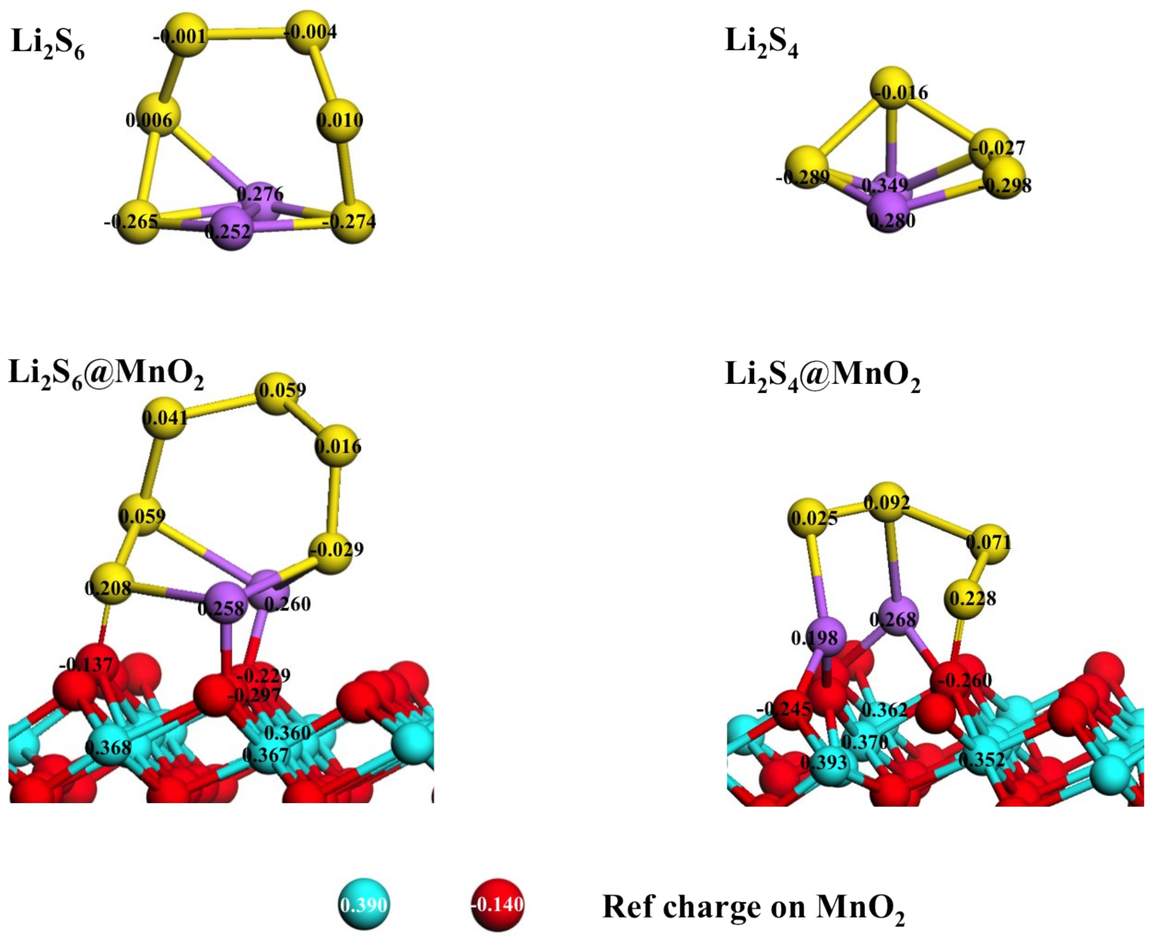

Supplymentary Figure 12. Hirshfeld charge analysis show that electrons were transferred from Li_2S_4 and Li_2S_6 species to MnO_2 support.

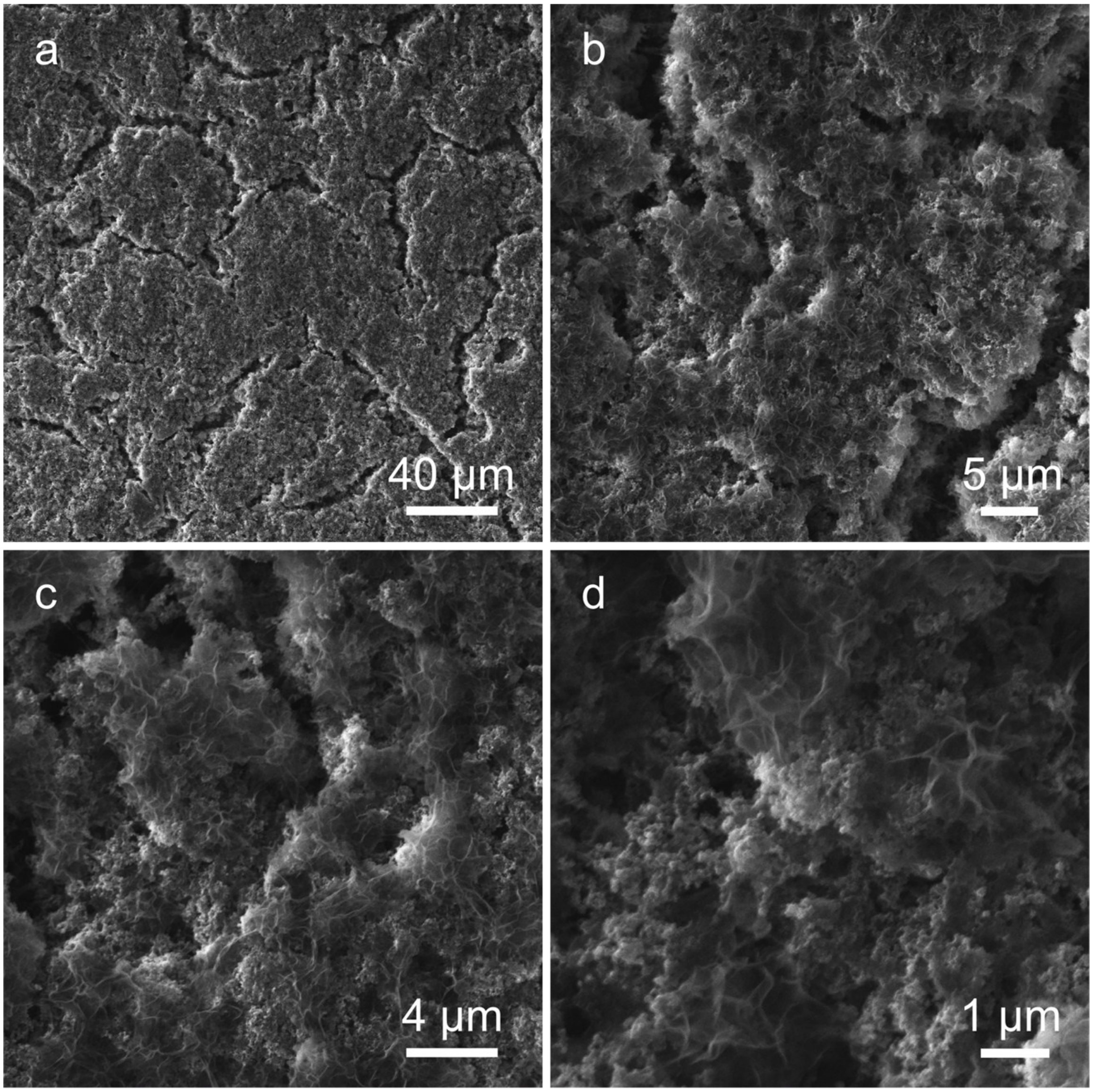

Supplymentary Figure 13. SEM images of the hollow S-MnO_2 nanocomposites electrode after cycling.

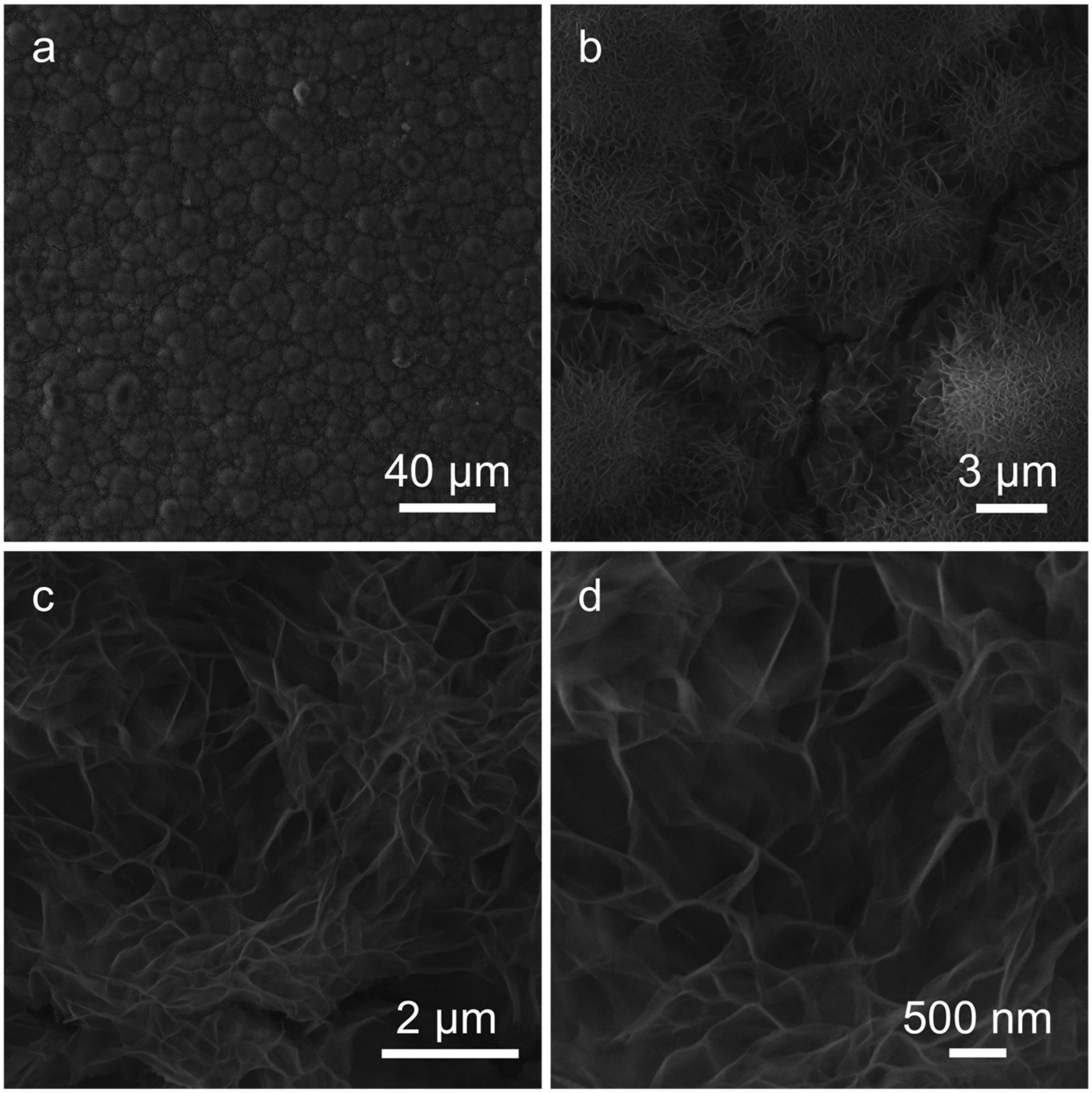

Supplymentary Figure 14. SEM images of the hollow S-MnO_2 nanocomposites electrode after cycling. The electrode was soaked in and washed by DOL to remove any lithium polysulfides.

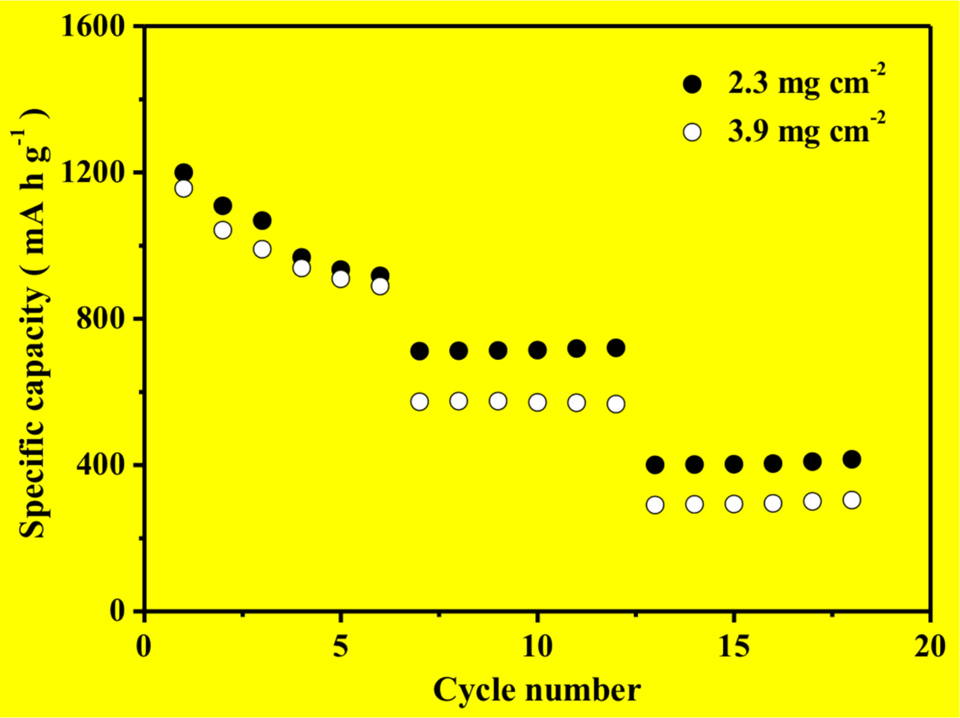

Supplymentary Figure 15. Rate performance of the hollow S-MnO$_2$ nanocomposites electrode at high mass loading of S.

References

[1] W. Li, G. Zheng, Y. Yang, Z. W. Seh, N. Liu, Y. Cui, *Proceedings of the National Academy of Sciences* **2013**, *110*, 7148.

[2] X. Liang, C. Hart, Q. Pang, A. Garsuch, T. Weiss, L. F. Nazar, *Nat Commun* **2015**, *6*.

[3] Q. Pang, D. Kundu, M. Cuisinier, L. F. Nazar, *Nat Commun* **2014**, *5*.

[4] G. Wiesenekker, E. J. Baerends, *Journal of Physics: Condensed Matter* **1991**, *3*, 6721.

[5] J. P. Perdew, K. Burke, M. Ernzerhof, *Physical Review Letters* **1996**, *77*, 3865.

[6] Q. Zhang, Y. Wang, Z. W. Seh, Z. Fu, R. Zhang, Y. Cui, *Nano Letters* **2015**, *15*, 3780.

[7] X.-Q. Gong, Z.-P. Liu, R. Raval, P. Hu, *Journal of the American Chemical Society* **2004**, *126*, 8.

[8] G. te Velde, E. J. Baerends, *Journal of Computational Physics* **1992**, *99*, 84.

[9] S. C. Modelling, Vol. 2015, 2015.

[10] S. C. Modelling, Vol. 2015, 2015.

[11] G. Wiesenekker, G. t. Velde, E. J. Baerends, *Journal of Physics C: Solid State Physics* **1988**, *21*, 4263.

[12] C. Barchasz, F. Molton, C. Duboc, J.-C. Leprêtre, S. Patoux, F. Alloin, *Analytical Chemistry* **2012**, *84*, 3973.

[13] J. E. Post, D. R. Veblen, *American Mineralogist* **1990**, *75*, 477.

[14] J. Li, E. Croiset, L. Ricardez-Sandoval, *The Journal of Physical Chemistry C* **2013**, *117*, 16907.

[15] M. C. Wu, C. A. Estrada, J. S. Corneille, D. W. Goodman, *The Journal of Chemical Physics* **1992**, *96*, 3892.

[16] E. M. Fernández, P. G. Moses, A. Toftelund, H. A. Hansen, J. I. Martínez, F. Abild-Pedersen, J. Kleis, B. Hinnemann, J. Rossmeisl, T. Bligaard, J. K. Nørskov, *Angewandte Chemie International Edition* **2008**, *47*, 4683.